NeuroImage: Clinical 30 (2021) 102608

Contents lists available at ScienceDirect

NeuroImage: Clinical

journal homepage: www.elsevier.com/locate/ynicl

Lateral geniculate nucleus volume changes after optic neuritis in neuromyelitis optica: A longitudinal study

Athina Papadopoulou [a,b,c,1], Frederike C. Oertel [a,b,d,1], Claudia Chien [a,b], Joseph Kuchling [a,b], Hanna G. Zimmermann [a,b], Nadja Siebert [a,b], Seyedamirhosein Motamedi [a,b], Marcus D' Souza [a,b,c], Susanna Asseyer [a,b], Judith Bellmann-Strobl [a,b], Klemens Ruprecht [e], M. Mallar Chakravarty [f,g], Michael Scheel [a,b,h], Stefano Magon [c,i], Jens Wuerfel [j], Friedemann Paul [a,b,e], Alexander U. Brandt [a,b,k,*]

[a] Experimental and Clinical Research Center, Max Delbrueck Center for Molecular Medicine and Charité – Universitätsmedizin Berlin, corporate member of Freie Universität Berlin, Humboldt-Universität zu Berlin, and Berlin Institute of Health, Berlin, Germany
[b] NeuroCure Clinical Research Center, Charité – Universitätsmedizin Berlin, corporate member of Freie Universität Berlin, Humboldt-Universität zu Berlin, and Berlin Institute of Health, Berlin, Germany
[c] Neurologic Clinic and Policlinic, Department of Medicine, Clinical Research and Biomedicine University Hospital Basel, University of Basel, Basel, Switzerland
[d] Department of Neurology, University of California San Francisco, CA, USA
[e] Department of Neurology, Charité – Universitätsmedizin Berlin, corporate member of Freie Universität Berlin, Humboldt-Universität zu Berlin, and Berlin Institute of Health, Berlin, Germany
[f] Cerebral Imaging Centre, Douglas Mental Health University Institute, Montreal, Canada
[g] McGill University, Department of Psychiatry and Department of Biomedical Engineering, Montreal, Canada
[h] Department of Neuroradiology, Charité – Universitätsmedizin Berlin, corporate member of Freie Universität Berlin, Humboldt-Universität zu Berlin, and Berlin Institute of Health, Berlin, Germany
[i] Pharma Research and Early Development, Roche Innovation Center Basel, F. Hoffmann-La Roche Ltd, Switzerland
[j] Medical Image Analysis Center (MIAC AG) and Department for Biomedical Engineering, Basel, Switzerland
[k] Department of Neurology, University of California Irvine, CA, USA

ARTICLE INFO

Keywords:
Thalamus
Neurodegeneration
NMOSD
Anterograde degeneration

ABSTRACT

Objectives: Lateral geniculate nucleus (LGN) volume is reduced after optic neuritis (ON) in neuromyelitis optica spectrum disorders (NMOSD). We aimed at a longitudinal assessment of LGN volume in NMOSD.
Methods: Twenty-nine patients with aquaporin 4-IgG seropositive NMOSD (age: 47.8 ± 14.6 years (y), female: n = 27, history of ON (NMO-ON): n = 17, median time since ON: 3[1.2–12.1]y) and 18 healthy controls (HC; age: 39.3 ± 15.8y; female: n = 13) were included. Median follow-up was 4.1[1.1–4.7]y for patients and 1.7[0.9–3.2]y for HC. LGN volume was measured using a multi-atlas-based approach of automated segmentation on 3 Tesla magnetic resonance images. Retinal optical coherence tomography and probabilistic tractography of the optic radiations (OR) were also performed.
Results: At baseline, NMO-ON patients had lower LGN volumes (395.4 ± 48.9 mm^3) than patients without ON (NMO-NON: 450.7 ± 55.6 mm^3; p = 0.049) and HC (444.5 ± 61.5 mm^3, p = 0.025). LGN volume was associated with retinal neuroaxonal loss and microstructural OR damage. Longitudinally, there was no change in LGN volumes in the absence of ON, neither in all patients (B = −0.6, SE = 1.4, p = 0.670), nor in NMO-ON (B = −0.8, SE = 1.6, p = 0.617) and NMO-NON (B = 1.7, SE = 3.5, p = 0.650). However, in four patients with new ON

Abbreviations: AD, axial diffusivity; AQP4, aquaporin-4; cR^2, conditional R^2; DTI, diffusion tensor imaging; EDSS, expanded disability status scale; FA, fractional anisotropy; GCIPL, ganglion cell-inner plexiform layer; LGN, lateral geniculate nucleus; mR^2, marginal R^2; MAGeT, Multiple Automatically Generated Templates; MD, mean diffusivity; MRI, magnetic resonance imaging; NMO-NON, patients with NMOSD and no prior optic neuritis; NMO-ON, patients with NMOSD and prior optic neuritis; NMOSD, neuromyelitis optica spectrum disorders; ON, optic neuritis; OR, optic radiations; pRNFL, peripapillary retinal nerve fiber layer; RD, radial diffusivity; SE, standard error.

* Corresponding author at: NeuroCure Clinical Research Center, Charité – Universitätsmedizin Berlin, Charitéplatz 1, DE-10117 Berlin, Germany.
E-mail address: alexander.brandt@charite.de (A.U. Brandt).

[1] These authors contributed equally.

https://doi.org/10.1016/j.nicl.2021.102608
Received 4 December 2020; Received in revised form 25 January 2021; Accepted 17 February 2021
Available online 4 March 2021

during follow-up, LGN volume was reduced at last visit (median time since ON: 2.6 [1.8–3.9] y) compared to the measurement before ON (352 ± 52.7 vs. 371.1 ± 55.9 mm^3; t = −3.6, p = 0.036).
Conclusion: Although LGN volume is reduced after ON in NMOSD, this volume loss is not progressive over longer follow-up or independent of ON. Thus, our findings -at least in this relatively small cohort- do not support occult neurodegeneration of the afferent visual pathway in NMOSD.

1. Introduction

Neuromyelitis optica spectrum disorders (NMOSD) are relapsing inflammatory disorders of the central nervous system (CNS) (Wingerchuk et al., 2015). Most patients with NMOSD (60–80%) have detectable serum antibodies binding to the water channel aquaporin-4 (AQP4–immunoglobulin G (IgG) seropositive NMOSD) (Lennon et al., 2004; Paul et al., 2007).

The afferent visual pathway is frequently affected in AQP4-IgG seropositive NMOSD, with optic neuritis (ON) being a typical clinical manifestation (Wingerchuk et al., 2015; Jarius et al., 2014; Borisow et al., 2018). The well-defined structure of the visual pathway, with its distinct nodes (retinal ganglion cells, optic nerve, lateral geniculate nucleus (LGN), optic radiation (OR) and primary visual cortex) makes it a suitable model to study pathological mechanisms of the disease (Pfueller and Paul, 2011; Oertel et al., 2018).

Previous studies in NMOSD assessed damage in the LGN and the OR via magnetic resonance imaging (MRI). It was shown, that patients with previous optic neuritis (NMO-ON) have smaller LGN volumes compared to patients without ON (NMO-NON) and to healthy controls (HC) (Papadopoulou et al., 2019; Tian et al., 2018). Moreover, microstructural changes in the OR of NMO-ON patients were described, using diffusion tensor and myelin water imaging (Tian et al., 2018; Pichiecchio et al., 2012; Manogaran et al., 2016; Oertel et al., 2017). These observations suggest anterograde transsynaptic degeneration along the afferent visual pathway of NMO-ON patients, resulting in LGN and OR damage (Papadopoulou et al., 2019; Tian et al., 2018; Pichiecchio et al., 2012; Manogaran et al., 2016; Oertel et al., 2017). Interestingly, OR changes were also observed in NMO-NON patients compared to HC (Tian et al., 2018; Oertel et al., 2017). However, these previous findings derived from cross-sectional studies.

Our objective was to assess the longitudinal course of LGN volume in AQP4-IgG seropositive NMOSD. We aimed at evaluating whether ongoing LGN volume loss occurs during the disease course or whether loss is solely associated to previous ON. Moreover, we aimed at quantifying the course of LGN volume change in patients presenting with new ON episodes during follow-up.

2. Materials and methods

2.1. Study participants

We screened 78 patients with NMOSD from an ongoing observational cohort study at the NeuroCure Clinical Research Center at Charité – Universitätsmedizin Berlin (recruited from May 2013 to January 2018). Inclusion criteria were: i) age ≥ 18 years, ii) AQP4-IgG seropositive NMOSD, according to the 2015 International Consensus Diagnostic Criteria (Wingerchuk et al., 2015) and iii) at least one clinical and MRI follow-up visit. AQP4-IgG seropositivity was determined by a cell-based assay (Euroimmun, Lübeck, Germany) (Jarius et al., 2014). Patients that were AQP4-IgG seronegative (n = 25), or had incomplete clinical data, or unknown AQP4-IgG-status (n = 10), or no follow-up MRI data (n = 11) were excluded. In order to avoid an influence of acute inflammatory activity on the analysis, we excluded visits of patients with an attack within six months before ths visit (n = 3 visits of 3 patients as well as 3 patients totally excluded, due to attacks within six months prior to every visit), except if the attack was a new ON during follow-up. Altogether, 29 patients were included in the analysis. It must be noted that visits of these patients (one visit of each) had been previously included in a cross-sectional analysis of the LGN in NMOSD (Papadopoulou et al., 2019).

At every visit, patients underwent a comprehensive neurological examination to assess the Expanded Disability Status Scale (EDSS),

Fig. 1. LGN segmentation by MAGeT. **Legend**: This figure is a representative lateral geniculate nucleus (LGN) segmentation in a control subject, as performed by the MAGeT brain algorithm (Chakravarty et al., 2013, 2006). The LGN is shown in red at: A) axial, B) coronal and C) sagittal view, on a 3D T1-weighted magnetization prepared rapid acquisition gradient echo (MPRAGE) sequence. (For interpretation of the references to colour in this figure legend, the reader is referred to the web version of this article.)

according to the Neurostatus definitions (Kappos et al., 2015). Attack history including ON was recorded using clinical criteria (Petzold et al., 2014).

Median follow-up for the patients was 4.1 years (range: 1.1–4.7); in particular patients with previous ON (NMO-ON) had a median follow-up of 4.2 years (range 1.1–4.7) and patients without previous ON (NMO-NON) had a median follow-up of 3.1 years (range 1.1–4.5).

Longitudinal data from 18 HC with age ≥ 18 years, at least one MRI follow-up, without a history of neurological or opthalmological diseases were also included. HC were chosen from the institute's research database, to be as well matched as possible with the patients' age and sex. Twelve of the HC had been also included in our previous cross-sectional analysis of the LGN in NMOSD (Papadopoulou et al., 2019). Median follow-up for the HC was 1.7 years (range: 0.9–3.2).

This study was approved by the local ethics committee (Ethikkommission der Charité – Universitätsmedizin Berlin; EA1/041/14 and EA1/163/12) and conducted in accordance with the declaration of Helsinki in its currently applicable version. All participants gave written informed consent before inclusion in the study.

2.2. Magnetic resonance imaging (MRI)

3 Tesla MRI was performed at every visit for all participants (MAGNETOM Trio Tim, Siemens, Erlangen, Germany). Details regarding the MRI protocol are given as Supplementary material.

2.3. Measurement of LGN volume

LGN volumes were measured at all timepoints using the Multiple Automatically Generated Templates (MAGeT) brain algorithm (Chakravarty et al., 2013) on isotropic 3D T1-weighted magnetization prepared rapid acquisition gradient echo (MPRAGE) images. MAGeT uses an atlas derived from manually segmented serial histological data, including delineation of the thalamic nuclei. It first customizes the atlas to a subset of participants, representative of the study population, using nonlinear registration and uses this newly segmented subset as a template library for the remaining participants. This has the advantage of correcting for the neuroanatomical variability of the study population (Chakravarty et al., 2013). Details regarding the representative subset of the present study are given as Supplementary material.

Segmentation results were visually inspected by one experienced rater (S.M.), who was blinded to the clinical data. No subjects had to be excluded. All volumes were normalised using the SIENAX V-scaling factor for head-size (Smith et al., 2002). In the analysis, we used the sum of the right and left LGN, defined as "total LGN volume".

An example of the LGN as segmented by MAGeT can be seen in Fig. 1.

2.4. Assessment of the OR microstructure

Diffusion tensor imaging (DTI)-based probabilistic tractography were used to assess the OR microstructure. The methodological details are given as Supplementary material. Tract profiles of weighted mean values of fractional anisotropy (FA), mean diffusivity (MD), radial diffusivity (RD), and axial diffusivity (AD) at 50 equally spaced positions of the OR were computed at all timepoints. The mean values of these 50 positions were used in the analysis.

Eight patients and four HC (total of 12 participants) did not have DTI-data at baseline (n = 9 due to failure of tract generation and n = 3 due to not available DTI-sequence).

2.5. Retinal optical coherence tomography (OCT)

Retinal imaging was performed for all participants, using a Heidelberg Engineering Spectralis spectral domain OCT (Heidelberg Engineering, Heidelberg, Germany). We report the OCT acquisition settings, scanning protocol and details regarding excluded scans as Supplementary material.

The mean peripapillary retinal nerve fiber layer (pRNFL) thickness and the mean combined ganglion cell and inner plexiform layer (GCIPL) thickness at baseline were used. The longitudinal OCT data of this cohort were previously published by our group as part of a multicenter study (Oertel et al., 2018).

Table 1
Baseline characteristics of the study participants.

Baseline characteristics	AQP4-IgG seropositive NMOSD (n = 29)	HC (n = 18)
Age, years (mean ± SD)	47.8 ± 14.6	39.3 ± 15.8
Sex: female/male (female %)	27/2 (93.1%)	13/5 (72.2%)
Handedness: right/left (righthanded %)	26/3 (89.7%)	18/0 (100%)
Race: Caucasian/African/Asian	27/1/1	18/0/0
Disease duration, years: median (range)	4.6 (0.5–28.0)	–
Follow-up time, years: median (range)	4.1 (1.1–4.7)	1.7 (0.9–3.2)
EDSS: median (range)	3.5 (1–6.5)	–
Patients on immunosuppressive treatment: n (%)	28 (96.6%)*	–
Total number of previous attacks: median (range)	3 (1–21)	–
Patients with myelitis: n (%)	27 (93.1%)	–
Patients with ON: n (%)	17 (58.6%)	–
Number of ON episodes per patient: median (range)	1 (0–7)	–
Time since fist ON episode, years: median (range)	4.6 (1.8–28.0)	–
Time since last ON episode, years: median (range)	3.0 (1.2–12.1)	–

Patients and HC showed no significant difference regarding mean age (t = −1.8, p = 0.076), sex (OR = 5.0, p = 0.089) or handedness (OR = 0, p = 0.276).
Abbreviations: AQP4-IgG = Aquaporin-4 immunoglobulin-G, EDSS = Expanded Disability Status Scale, HC = healthy controls, NMOSD = neuromyelitis optica spectrum disorders, ON = optic neuritis, SD = standard deviation.
* The only untreated patient at baseline had previous treatment with cyclophoshamid until 4 years before study-baseline but did not receive any permanent immunomodulatory/immunosuppressive treatment during the study.

2.6. Statistical analysis

Differences at baseline characteristics between patients and HC were investigated using *t*-test (age), Fisher's exact test (sex- and handedness-distribution) and analysis of covariance (ANCOVA model Type III with adjustment for age and sex to compare baseline OCT- and DTI-measures among: NMO-ON, NMO-NON and HC).

Total LGN volume at baseline was also compared among these three groups using ANCOVA. Moreover, the associations between total LGN volume and other measures of the visual pathway (pRNFL, GCIPL, OR-FA, OR-MD, OR-RD and OR-AD; in all cases mean of both eyes/hemispheres) were examined in linear regression models with adjustment for age and sex.

For the longitudinal analysis, linear mixed effect models (LMM) were used. To study the course of total LGN volume over time in the different groups (NMOSD, NMO-ON, NMO-NON, HC), we used a LMM with fixed effects: time since baseline, age and sex and random effects based on subject and visit (total LGN volume ~ time since baseline + age + sex + (1 |time since baseline|subject)). For the NMO-ON subgroup we also performed two LMM using time since first- and last ON episode, instead of time since baseline.

To study group-differences in the course of total LGN volume, we used a LMM with fixed effects: the interaction between time since baseline and group, as well as age and sex, and random effects based on subject and visit (total LGN volume ~ time since baseline × group + age + sex + (1 |time since baseline|subject)). From all models, patients with

Table 2
Cross-sectional group-comparisons of OCT- and DTI-measures.

	NMO-ON	NMO-NON	HC	ANCOVA	NMO-ON vs. NMO-NON	NMO-ON vs. HC	NMO-NON vs. HC
Mean pRNFL thickness at baseline, μm	72.3 ± 20.5 (n = 15)	98.5 ± 12.2 (n = 12)	95.6 ± 11.3 (n = 17)	F = 12.30 p < 0.001	**B = −26.9 (SE = 6.4) p < 0.001**	**B = –23.3 (SE = 5.8) p < 0.001**	B = 3.6 (SE = 6.8) p = 0.862
Mean GCIPL thickness at baseline, μm	62.0 ± 10.3 (n = 15)	76.7 ± 5.1 (n = 11)	78.7 ± 7.1 (n = 17)	F = 18.29 p < 0.001	**B = −15.4 (SE = 3.3) p < 0.001**	**B = −16.3 (SE = 3.1) p < 0.001**	B = −0.9 (SE = 3.6) p = 0.965
Mean OR-FA at baseline	0.484 ± 0.03 (n = 11)	0.505 ± 0.03 (n = 10)	0.510 ± 0.03 (n = 14)	F = 2.32 p = 0.116	B = −0.03 (SE = 0.01) p = 0.133	B = −0.02 (SE = 0.01) p = 0.254	B = 0.01 (SE = 0.01) p = 0.887
Mean OR-MD at baseline	0.941 ± 0.10 (n = 11)	0.90 ± 0.07 (n = 10)	0.955 ± 0.09 (n = 14)	F = 1.51 p = 0.238	B = 0.05 (SE = 0.04) p = 0.463	B = −0.02 (SE = 0.04) p = 0.814	B = −0.07 (SE = 0.04) p = 0.214
Mean OR-RD at baseline	0.688 ± 0.11 (n = 11)	0.635 ± 0.07 (n = 10)	0.685 ± 0.09 (n = 14)	F = 1.48 p = 0.244	B = 0.06 (SE = 0.04) p = 0.335	B = −0.01 (SE = 0.04) p = 0.972	B = −0.07 (SE = 0.04) p = 0.260
Mean OR-AD at baseline	1.447 ± 0.10 (n = 11)	1.418 ± 0.06 (n = 10)	1.494 ± 0.11 (n = 14)	F = 1.76 p = 0.190	B = 0.03 (SE = 0.04) p = 0.781	B = −0.05 (SE = 0.04) p = 0.415	B = −0.08 (SE = 0.05) p = 0.181
Mean OR-FA at last visit	0.468 ± 0.04 (n = 17)	0.507 ± 0.03 (n = 11)	0.514 ± 0.03 (n = 16)	F = 7.15 p = 0.002	**B = −0.04 (SE = 0.01) p = 0.014**	**B = −0.04 (SE = 0.01) p = 0.007**	B = −0.0003 (SE = 0.02) p > 0.999
Mean OR-MD at last visit	1.022 ± 0.17 (n = 17)	0.888 ± 0.06 (n = 11)	0.940 ± 0.10 (n = 16)	F = 4.05 p = 0.025	**B = 0.12 (SE = 0.05) p = 0.041**	B = 0.09 (SE = 0.04) p = 0.104	B = −0.03 (SE = 0.05) p = 0.860
Mean OR-RD at last visit	0.771 ± 0.18 (n = 17)	0.627 ± 0.06 (n = 11)	0.670 ± 0.10 (n = 16)	F = 4.77 p = 0.014	**B = 0.13 (SE = 0.05) p = 0.029**	B = 0.11 (SE = 0.05) p = 0.058	B = −0.02 (SE = 0.06) p = 0.903
Mean OR-AD at last visit	1.524 ± 0.16 (n = 17)	1.410 ± 0.08 (n = 11)	1.479 ± 0.11 (n = 16)	F = 2.40 p = 0.104	B = 0.10 (SE = 0.05) p = 0.111	B = 0.06 (SE = 0.04) p = 0.350	B = −0.04 (SE = 0.05) p = 0.772

For all measures the mean ± standard deviation is shown; they all represent the mean of both sides (for OCT-measures: both eyes and for DTI-measures: both cerebral hemispheres). Note that due to reduced number of participants with baseline DTI-data (n = 12 missing), we also performed the cross-sectional group comparisons at the last follow-up visit (only n = 3 missing). These results are shown below the baseline DTI- results ("at last visit"). Significant results are marked in bold.
Abbreviations: AQP4-IgG = Aquaporin-4 immunoglobulin-G, DTI = diffusion-tensor imaging, GCIPL = ganglion cell-inner plexiform layer, HC = healthy controls, NMO-NON: patients without previous optic neuritis, NMO-ON = patients with previous optic neuritis, OCT = optical coherence tomography, ON = optic neuritis, OR-AD: axial diffusivity of the optic radiations, OR-FA: fractional anisotropy of the optic radiations, OR-MD = mean diffusivity of the optic radiations, OR-RD: radial diffusivity of the optic radiations, pRNFL = peripapillary retinal nerve layer

new ON episodes during follow-up were excluded.

To analyse the course of total LGN volume change for patients with new ON during follow-up, we used a paired *t*-test, since the number of these patients was too low to perform LMM (n = 4). We compared total LGN volume between: i) V0 (last visit before new ON) and V1 (first visit after new ON), and ii) V0 and Vlast (last available visit). As a control-analysis, we performed the same paired t-tests in four patients without new ON during follow-up, who were matched to the patients with new ON regarding relevant characteristics (such as age, sex, race, prior ON, etc.).

For all models, statistical significance was set at $p < 0.05$. All statistical analysis was performed using R version 3.4.3 (R Core Team, 2017) with packages: pastecs, compute.es, car, effects, multcomp, stats, WRSS, lme4, lmerTest, MuMIn, Matrix and ggplot2.

2.7. Data availability statement

All fully anonymised data that were used in the analysis can be shared upon reasonable request from qualified investigators.

3. Results

3.1. Baseline characteristics of the study participants

The baseline demographics and clinical characteristics of the study participants are summarized in Table 1.

The imaging characteristics (OCT- and DTI-measures) of NMO-ON, NMO-NON patients and HC at baseline are summarized in Table 2. The OCT-measures showed significant group differences at baseline: between NMO-ON and NMO-NON, as well as between NMO-ON and HC (Table 2). In contrast, there were no baseline group-differences regarding the DTI-measures (Table 2). Since we suspected that this might be attributed to reduced power due to many subjects without baseline DTI data (n = 12), we also performed a group comparison of the DTI measures at the last follow-up visit, where only 3 subjects had no DTI data (using again the same ANCOVA models as at baseline). At this time-point, we indeed found significant group-differences in OR-FA, OR-MD and OR-RD (Table 2).

3.2. LGN volume at baseline

At baseline, mean total LGN volume was 444.5 ± 61.5 mm^3 in HC, 450.7 ± 55.6 mm^3 in NMO-NON patients and 395.4 ± 48.9 mm^3 in NMO-ON patients. In an analysis of covariance with adjustment for age and sex, total LGN volume was associated with group (HC vs. NMO-NON vs. NMO-ON; F = 4.89, p = 0.012).

In detail, NMO-ON patients had lower volumes compared to HC (B = −53.2, SE = 19.6, 95% CI: −53.2 to −100.8, t = −2.7, p = 0.025) and to NMO-NON patients (B = −53.0, SE = 21.7, 95% CI: −53.0 to −105.8, t = −2.4, p = 0.049), while NMO-NON patients did not differ from HC (B = −0.2, SE = 23.4, 95% CI: −56.9 to 56.6, t = −0.007, p > 0.99).

Moreover, total LGN volume at baseline was associated with measures of neuroaxonal loss in the retina (mean pRNFL and GCIPL thicknesses) and of microstructural damage in the OR (mean OR-FA, OR-MD, OR-RD and OR-AD; Table 3 and Fig. 2).

In a subgroup analysis, most associations remained in the NMO-ON patients (Table 3), while there were no associations in the NMO-NON subgroup and in HC (Table 3).

Table 3
Associations between total LGN volume and measures of damage in the retina and the OR at baseline.

Total LGN volume	Mean pRNFL thickness	Mean GCIPL thickness	Mean OR-FA	Mean OR-MD	Mean OR-RD	Mean OR-AD
NMOSD	**B = 1.9**	**B = 3.7**	**B = 1018.2**	**B = −455.1**	**B = −417.0**	**B = −468.7**
	SE = 0.5	**SE = 1.0**	**SE = 358.0**	**SE = 121.5**	**SE = 118.4**	**SE = 125.8**
	p < 0.001	**p < 0.001**	**p = 0.011**	**p = 0.002**	**p = 0.003**	**p = 0.002**
NMO-ON	**B = 1.9**	B = 2.6	B = 762.6	**B = −367.9**	**B = −328.7**	**B = −404.6**
	SE = 0.6	SE = 1.4	SE = 502.5	**SE = 128.0**	**SE = 134.3**	**SE = 112.2**
	p = 0.006	p = 0.086	p = 0.173	**p = 0.024**	**p = 0.044**	**p = 0.009**
NMO-NON	B = −0.6	B = 2.1	B = 810.6	B = −436.4	B = −388.1	B = −441.3
	SE = 1.4	SE = 3.5	SE = 587.5	SE = 268.7	SE = 254.2	SE = 279.4
	p = 0.657	p = 0.553	p = 0.210	p = 0.148	p = 0.171	p = 0.158
HC	B = 1.2	B = 2.0	B = 1130.6	B = −155.6	B = −186.2	B = −99.0
	SE = 1.7	SE = 3.1	SE = 771.8	SE = 205.4	SE = 217.7	SE = 174.9
	p = 0.483	p = 0.538	p = 0.171	p = 0.465	p = 0.411	p = 0.583

The different columns show the associations of total LGN volume with the different measures of damage in the retina (mean pRNFL and GCIPL thicknesses) and the OR (mean OR-FA, mean OR-MD, mean OR-RD, mean OR-AD) at baseline. The different rows represent the analysis in the entire patient group (NMOSD), the subgroup with previous ON (NMO-ON), the subgroup without previous ON (NMO-NON) and the healthy controls (HC). Significant associations are marked in bold.
Abbreviations: AD = axial diffusivity, AQP4 = aquaporin 4, B = beta estimate of the linear mixed effect models, GCIPL: ganglion cell-inner plexiform layer, FA = fractional anisotropy, LGN = lateral geniculate nucleus, MD = mean diffusivity, NMO-NON: patients without history of optic neuritis, NMO-ON: patients with positive history of optic neuritis, NMOSD = neuromyelitis optica spectrum disorders, pRNFL = peripapillary retinal nerve fiber layer, OR = optic radiation, RD = radial diffusivity, SE = standard error of the B.

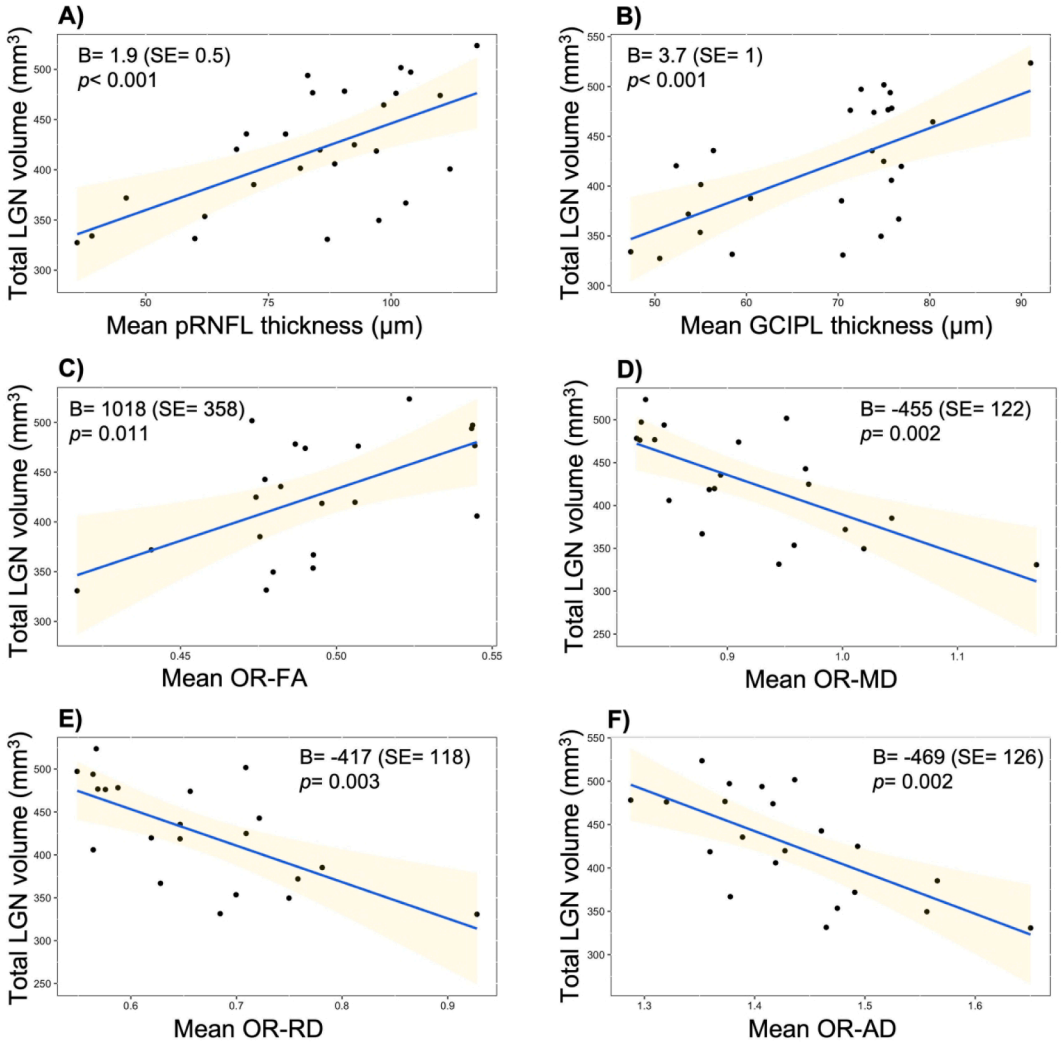

Fig. 2. Cross-sectional associations between total LGN volume and other measures of structural damage in the visual pathway. **Legend**: At baseline, total LGN volume of AQP4 IgG seropositive NMOSD patients was associated with the measures of neuroaxonal loss in the retina: A) mean pRNFL thickness, and B) mean GCIPL thickness, as well as with the measures of microstructural damage in the optic radiations: C) mean OR-FA, D) mean OR-MD, E) mean OR-RD and F) mean OR-AD. **Abbreviations**: AD = axial diffusivity, GCIPL: ganglion cell-inner plexiform layer, FA = fractional anisotropy, LGN = lateral geniculate nucleus, MD = mean diffusivity, pRNFL = peripapillary retinal nerve fiber layer, OR = optic radiation, RD = radial diffusivity, SE = standard error.

3.3. Longitudinal course of LGN volume

3.3.1. Patients without new ON during follow-up

After exclusion of four patients that showed new ON episodes during follow-up, we examined the longitudinal course of total LGN volume in the cohort. We found no change in total LGN volume over time, neither in all remaining patients (B = −0.6, SE = 1.4, p = 0.670), nor in the NMO-ON (B = −0.8, SE = 1.6, p = 0.617) and NMO-NON subgroups (B = 1.7, SE = 3.5, p = 0.650). In the NMO-ON subgroup the results did not change when evaluating the length of time since an ON attack rather than the duration since baseline in the analysis (results for time since first ON episode: B = 0.8, SE = 0.8, p = 0.425; results for time since last ON episode: B = 0.2, SE = 1.5, p = 0.910). It should be noted that in HC (shorter follow-up time compared to patients: median 1.7 years) there was also no significant total LGN volume change during this study (B = −3.8, SE = 3.6, p = 0.304). Moreover, there was no group effect on the course of total LGN volume change (Fig. 3).

In line with the LGN-results, there was also no change in the course of DTI-metrics over time in the defined groups (all patients without new ON, NMO-ON and NMO-NON; data not shown).

3.3.2. New ON during follow-up: a case series of four patients

Four patients suffered new ON episodes during follow-up, all of whom already had ON episodes prior to baseline (NMO-ON). The new ON episodes were unilateral for three patients (n = 2 on the right and n = 1 on the left eye), while one patient (P4) suffered one episode of bilateral ON and an additional episode of left ON one month later.

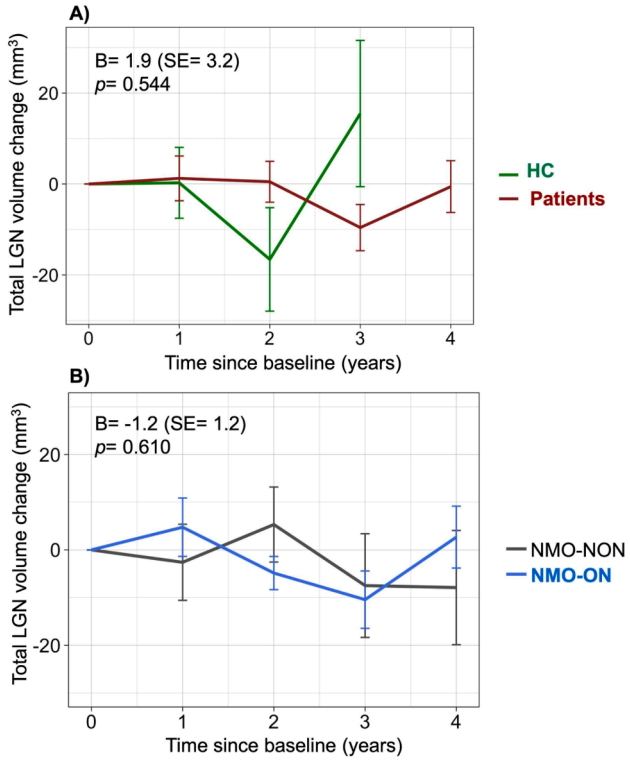

Fig. 3. Course of total LGN volume during the study in different groups/subgroups. **Legend**: There was no significant change in total LGN volume during follow-up in any groups (HC, all patients, NMO-ON, NMO-NON). Moreover, there was no group effect on LGN volume change: A) neither between HC and all AQP4-IgG seropositive NMOSD patients; B) nor between NMO-NON and NMO-ON patients. Note that the y axis represents the change in total LGN volume (sum of right and left) and not the absolute volumes. Moreover, note that there were only 9 HC with 2- and 3 HC with 3 years follow-up, which at least partly explains the higher variance in LGN volume change seen in HC, as shown in A. **Abbreviations**: HC = healthy controls, LGN = lateral geniculate nucleus, NMO-NON: patients with NMOSD and no prior optic neuritis, NMO-ON: patients with NMOSD and prior optic neuritis, SE = standard error.

Table 4
Course of total LGN volume in four patients with new ON during follow-up and in four "control"-patients.

4i) Patients with new ON during follow-up	Total LGN volume (sum of right and left), mm^3 (time since new ON, y)		
	V0	V1	Vlast
P1	327.4 (−0.8y)	332.0 (+1.8y)	310.6 (+3.9y)
P2	451.0 (−0.4y)	451.3 (+0.9y)	422.5 (+2.8y)
P3	367.5 (−0.2y)	391.8 (+0.8y)	362.2 (+1.8y)
P4	338.5 (−1.1y)	350.4 (+0.2y)	312.7 (+2.3y)
Mean ± SD of P1-P4	**371.1 ± 55.9** *	381.4 ± 52.9	**352 ± 52.7** *
4ii) Four matched "negative controls"-patients without new ON during follow-up	**Total LGN volume (sum of right and left), mm^3**		
	V0	**V1**	**Vlast**
CP1	442.7	431.7	415.5
CP2	420.4	405.1	419.9
CP3	331.5	329.0	340.2
CP4	385.2	421.2	405.4
Mean ± SD of CP1-CP4	394.9 ± 48.5	396.8 ± 46.5	395.2 ± 37.2

For the patients with new ON during follow-up, V0 was the last visit before the new ON episode, while V1, and Vlast were visits after the new ON episode. For the matched patients without new ON during follow-up, V0 was the baseline visit and Vlast the last available visit. Note that P3 had only a total of two visits after the new ON episode, thus V2 is at the same time the last available visit (Vlast). Similarly, for CP3 V2 is at the same time Vlast. In patients with new ON, the difference between Vlast and V0 was significant (p = 0.036), while there was no difference between V1 and V0. In four patients without new ON that were as well matched as possible to the four patients with new ON, there were no differences in total LGN volume between visits.
Abbreviations: LGN = lateral geniculate nucleus, ON = optic neuritis, SD = standard deviation.

The total LGN volumes of these four patients at different visits are shown in Table 4 and Fig. 4.

There was no difference in total LGN volume between V1 (median time since new ON: 1.3 years with range 1.0 to 2.6) and V0 (t = 2.0, p = 0.144, mean difference: 10.3 mm^3, with 95% CI: −6.4 to 27.0). However, at Vlast (median time since new ON: 2.6 years with range: 1.8 to

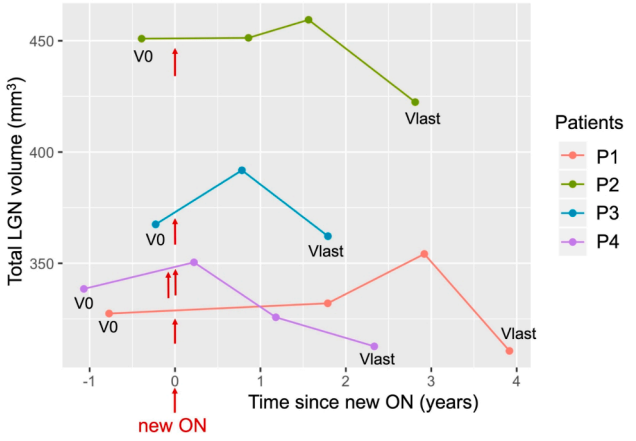

Fig. 4. LGN volume course in four patients with new ON during follow-up Legend: V0 is for all patients the last visit before the new ON episode and Vlast the last available visit. The time of new ON episodes is indicated with the red arrows. Note that patients P1-P3 had only one new ON episode, while P4 had two new episodes, with one month interval inbetween. In a paired *t*-test, mean LGN volume (sum of both hemispehres) was reduced in these four patients at Vlast compared to V0 (see also Table 4). Abbreviations: LNG = lateral geniculate nucleus, ON = optic neuritis. (For interpretation of the references to colour in this figure legend, the reader is referred to the web version of this article.)

3.9 years) we found a significant decrease in total LGN volume compared to V0 (t = −3.6, p = 0.036, mean difference: −19.1, with 95% CI: −35.8 to −2.4) (Table 4i). This volume change was specific for the LGN, since the total thalamic volume did not differ between Vlast and V0 (t = 0.4, p = 0.713, mean difference: 43.9, with 95% CI: −302.1 to 390.1).

For comparison, we examined the course of total LGN volume in four patients that did *not* show new ON episodes during follow-up ("negative controls"). We chose these patients -blinded to their LGN volumes- to be as well matched as possible to the four patients with new ON (for details see also Table S1). In this analysis, we did not find any change in total LGN volume between V1 and V0 (t = −0.2, p = 0.887, mean difference: −1.8, with 95% CI −39.1 to 35.4), nor between Vlast and V0 (median follow-up: 4.1 years with range 3.4 to 4.2; t = −0.03, p = 0.979, mean difference: −0.29, with 95% CI –32.5 to 31.9) (Table 4ii).

4. Discussion

In the current study, we examined longitudinal quantitative changes in the LGN of patients with AQP4-IgG seropositive NMOSD. Our cross-sectional findings at baseline, with reduced LGN volumes in NMO-ON patients, are in line with two previous studies, one from our own group (Papadopoulou et al., 2019; Tian et al., 2018). Here, we additionally observed significant cross-sectional associations between the LGN volume and other measures of structural damage along the visual pathway: i) neuroaxonal loss in the retina, as measured by OCT, and ii) microstructural damage in the OR, as measured by DTI. Most of these associations remained significant only in the NMO-ON-subgroup, suggesting that they were driven by prior ON. In line with this, we observed a reduction in total LGN volume of four patients showing *new* ON during follow-up. Overall, these results support the occurrence of anterograde trans-synaptic degeneration after ON in AQP4-IgG seropositive NMOSD.

Moreover, our findings underline the role of LGN volume as a marker of ON-related damage in the afferent visual pathway of these patients, which is also associated with visual function, according to our previous study (Papadopoulou et al., 2019). LGN volume as marker also has the advantage of its utility with a widely available MRI sequence (MPRAGE). The latter is relevant, since other measures of structural damage in the visual pathway (pRNFL- and GCIPl-thickness, mean FA and MD of the OR) require either OCT- or DTI, which are often not available in regular clinical practice (Papadopoulou et al., 2019).

In contrast to the above-mentioned results, we did not find progressive LGN volume loss in patients that did *not* suffer new ON episodes during follow-up. Although our small sample size may limit the generalizability of our results, this argues against occult neurodegenerative damage along the visual pathway in AQP4-IgG seropositive NMOSD, which is also suggested by the normal baseline LGN volumes of NMO-NON patients.

Although longitudinal MRI data in NMOSD are very limited, the absence of progressive neurodegeneration over time is in line with previous findings. One study with 18 AQP4-IgG-seropositive NMOSD patients and 15 patients with relapsing-remitting (RR)MS examined changes in volumetric and microstructural brain measures over time (Matthews et al., 2015). Overall, NMOSD patients did not show any changes over one-year follow-up (no reduction in brain and thalamic volume, no changes in the FA of normal appearing white matter, or the myelin water imaging of the brain). This was in contrast to the changes observed in the MS group, including a decrease in thalamic volume and FA reduction in multiple white matter regions (Matthews et al., 2015). A subgroup of patients in this previous study also underwent myelin-water imaging of their cervical spinal cord (Combes et al., 2017), which showed reduced myelin water fraction in lesional and non-lesional cervical cord areas of NMOSD patients at baseline, but no changes over one year follow-up, in contrast to MS patients, which showed a decrease (Combes et al., 2017).

This previous study highlights the differences between AQP4-IgG-seropositive NMOSD and MS regarding the mechanisms of neurodegeneration. On one hand, attack-related remote neurodegeneration, as in anterograde trans-synaptic degeneration after optic neuritis, seems to occur both in NMO-ON (Papadopoulou et al., 2019; Tian et al., 2018; Pichiecchio et al., 2012; Manogaran et al., 2016; Oertel et al., 2017) and in MS (Papadopoulou et al., 2019; Balk et al., 2015; Gabilondo et al., 2014; Ciccarelli et al., 2005; Audoin et al., 2006; Rocca et al., 2013). On the other hand, subclinical ongoing neurodegeneration independently of attacks and/or lesions is probably a hallmark of MS and not AQP4-IgG-seropositive NMOSD. Several studies have shown progressive neurodegeneration measured as grey matter atrophy in patients with MS, which is at least partially independent of focal lesions (Calabrese et al., 2015). Although its mechanisms are still not completely understood and probably combine both degenerative (e.g. neuroaxonal damage due to mitochondrial dysfunction) and inflammatory pathways (Calabrese et al., 2015); grey matter damage in MS is believed to be strongly associated to progression (Stadelmann, 2011). Thus, the lack of progressive deep grey matter damage in AQP4-IgG-seropositive NMOSD suggested by our current and previous findings (normal volumes of deep grey matter structures (Finke et al., 2016) and of other thalamic nuclei than the LGN (Papadopoulou et al., 2019) would be in line with the clinical observation, that progression in NMOSD is extremely rare (Wingerchuk et al., 2007).

However, there are also some contradictory findings regarding subclinical neuroaxonal damage in NMOSD. For example, previous studies -also from our group- showed reduced GCIPL volumes (Oertel et al., 2018) and microstructural OR changes (Oertel et al., 2017) in AQP4-IgG seropositive NMOSD, even *without* prior ON. Moreover, a longitudinal analysis of OCT-data in these patients (Oertel et al., 2018) revealed GCIPL loss over time, without new ON attacks. The reasons for this discrepancy are not clear. It could be that neurodegenerative processes are different in the brain vs. retina in NMOSD, with a primary retinopathy being potentially responsible for occult GCIPL loss. Moreover, retrograde degeneration due to contralateral ON with chiasmal affection could play a role in the GCIPL loss of non-ON eyes (Oertel et al., 2018), since in this previous study non-affected eyes of patients with unilateral ON were included.

Last, it cannot be ruled out that we had insufficient power to detect subtle subclinical volume loss at the LGN level in the current longitudinal analysis. This might be due to the relatively low number of patients included in the study, particularly in the NMO-NON subgroup (n = 12).

In this regard, there is need for larger studies, and at the same time, for robust MRI-markers reflecting structural damage in the visual pathway of patients with NMOSD. The LGN volume might be such a marker. Most previous studies assessing LGN volume in healthy volunteers (Fujita et al., 2001; Kitajima et al., 2015), patients with glaucoma (Dai et al., 2011; Chen et al., 2013; Furlanetto et al., 2018) and patients with NMOSD (Tian et al., 2018) used manual segmentation, which is time-consuming and probably inacurate for such a small grey matter structure (Magon et al., 2014). In our current and previous NMOSD-study (Papadopoulou et al., 2019), the LGN volume was measured using an atlas-based tool of automated segmentation of the thalamic nuclei, the MAGeT Brain algorithm (Chakravarty et al., 2006). MAGeT was validated against manual segmentations (Chakravarty et al., 2009), intraoperative recordings (Chakravarty et al., 2008) and functional MRI (Chakravarty et al., 2009). It was previously used to show LGN volume loss in patients with MS compared to controls (Papadopoulou et al., 2019). It has the advantages of automated vs. manual segmentation regarding rapidity and reliability, with also reduction of random errors. The latter is achieved by using a representative subgroup of the study population to create a template library and generate multiple segmentations of all other MRIs. This approach may be also useful to address the potential limitation of MAGeT in a longitudinal analysis, relating to the variability across MRI scans due to physiological or methodological factors. This limitation might be particularly problematic in the analysis of small structures like the LGN. The use of the template library, where

MRI sessions are sampled from all timepoints to be representative of possible changes over time additionally to demographic and clinical characteristics of the study population, should reduce this bias (Magon et al., 2020). A previous longitudinal analysis using MAGeT in MS showed correlations between volume loss of multiple thalamic nuclei (including the LGN) with the EDSS and -for three nuclei- with EDSS change over time. The latter was shown for example for the anterior nucleus, which had a similar volume to the LGN (Magon et al., 2020), suggesting that MAGeT can measure clinically meaningful changes over time even in small nuclei. However, it must be noted that -when looking at single patients- there is a considerable measurement variability in total LGN volume among different visits, which is restrictive in the use of this MRI marker at an individual level. In line with this, as also seen in the group of HC in the current study (see Fig. 3), the variability in the LGN volume measurement increases in small groups, which is an additional methodological limitation especially for small cohorts, as also in the current study. Thus, it is possible that the lack of LGN volume loss over time in the current study may be due to its relatively low power, since subtle volume changes may remain undetected in an analysis with small sample size and thus large measurement variability.

The main limitation of our study is indeed the relatively small number of patients. The sample size was particularly small in the subgroup of patients with new ON during follow-up (n = 4). Given the currently low annual relapse rates under immunosuppressive therapy, larger-potentially multicenter-studies are needed to further examine and confirm the temporal evolution of LGN volume after a (new) ON attack and its potential relevance for visual function. In this regard, it would be also interesting to investigate whether the small volume increase we observed at visit 1 after new ON (n.s.) is indeed a real phenomenon, or only artefact due to our small number of patients with new ON.

On the other hand, the inclusion of a well characterized cohort of AQP4-IgG seropositive NMOSD patients and the longitudinal analysis are strengths of this study. Moreover, we combined several methods for a comprehensive structural assessment of the afferent visual pathway: OCT for the retinal neuroaxonal integrity, DTI for the OR-microstructure and MAGeT for the LGN (Chakravarty et al., 2013). Through this combination we could show that LGN is not only smaller in NMO-ON, but also associated both with the retina- and OR-measures, confirming a cascade of damage along different parts of the visual pathway that are anatomically connected.

5. Conclusions

To conclude, despite reduced LGN volume in NMO-ON patients at baseline, we did not find subsequent LGN atrophy in the absence of new ON episodes. This suggests that LGN atrophy due to trans-synaptic degeneration in NMOSD occurs after ON but is not progressive over long-term follow-up, or independent of ON attacks. Our findings favour ON attack-related rather than occult neurodegenerative processes in AQP4-IgG seropositive NMOSD. Moreover, they underline the role of LGN volume as a marker of ON-associated structural damage, with the advantage of automated measurement on widely available MRI sequences.

Funding

This study was supported by the “Deutsche Forschungsgemeinschaft” (grant DFG EXC-257 and EXC-2049) and the German Federal Ministry for Education and Research (BMBF; grant N2-ADVISIMS: 16GW0079) to F.P. and A.U.B. and by the Swiss National Science Foundation (project number P300PB_174480) to A.P.

Declaration of Competing Interest

The authors declare that they have no known competing financial interests or personal relationships that could have appeared to influence the work reported in this paper.

Acknowledgments

We thank all patients and controls that participated in this study, Charlotte Bereuter for performing the visual assessment and optical coherence tomography, as well as Susan Pikol and Cynthia Kraut for performing the magnetic resonance imaging.

Appendix A. Supplementary data

Supplementary data to this article can be found online at https://doi.org/10.1016/j.nicl.2021.102608.

References

Audoin, B., Fernando, K.T.M., Swanton, J.K., Thompson, A.J., Plant, G.T., Miller, D.H., 2006. Selective magnetization transfer ratio decrease in the visual cortex following optic neuritis. Brain J. Neurol. 129 (4), 1031–1039. https://doi.org/10.1093/brain/awl039.

Balk, L.J., Steenwijk, M.D., Tewarie, P., Daams, M., Killestein, J., Wattjes, M.P., Vrenken, H., Barkhof, F., Polman, C.H., Uitdehaag, B.M.J., Petzold, A., 2015. Bidirectional trans-synaptic axonal degeneration in the visual pathway in multiple sclerosis. J. Neurol. Neurosurg. Psychiatry 86 (4), 419–424. https://doi.org/10.1136/jnnp-2014-308189.

Borisow, N., Mori, M., Kuwabara, S., Scheel, M., Paul, F., 2018. Diagnosis and treatment of NMO spectrum disorder and MOG-encephalomyelitis. Front. Neurol. 9 https://doi.org/10.3389/fneur.2018.00888.

Calabrese, M., Magliozzi, R., Ciccarelli, O., Geurts, J.J.G., Reynolds, R., Martin, R., 2015. Exploring the origins of grey matter damage in multiple sclerosis. Nat. Rev. Neurosci. 16 (3), 147–158. https://doi.org/10.1038/nrn3900.

Chakravarty, M.M., Bertrand, G., Hodge, C.P., Sadikot, A.F., Collins, D.L., 2006. The creation of a brain atlas for image guided neurosurgery using serial histological data. NeuroImage 30 (2), 359–376. https://doi.org/10.1016/j.neuroimage.2005.09.041.

Chakravarty, M.M., Sadikot, A.F., Germann, J., Bertrand, G., Collins, D.L., 2008. Towards a validation of atlas warping techniques. Med. Image Anal. 12 (6), 713–726. https://doi.org/10.1016/j.media.2008.04.003.

Chakravarty, M.M., Sadikot, A.F., Germann, J., Hellier, P., Bertrand, G., Collins, D.L., 2009. Comparison of piece-wise linear, linear, and nonlinear atlas-to-patient warping techniques: analysis of the labeling of subcortical nuclei for functional neurosurgical applications. Hum. Brain Mapp. 30 (11), 3574–3595. https://doi.org/10.1002/hbm.v30:1110.1002/hbm.20780.

Chakravarty, M.M., Rosa-Neto, P., Broadbent, S., Evans, A.C., Collins, D.L., 2009. Robust S1, S2, and thalamic activations in individual subjects with vibrotactile stimulation at 1.5 and 3.0 T. Hum. Brain Mapp. 30 (4), 1328–1337. https://doi.org/10.1002/hbm.v30:410.1002/hbm.20598.

Chakravarty, M.M., Steadman, P., van Eede, M.C., Calcott, R.D., Gu, V., Shaw, P., Raznahan, A., Collins, D.L., Lerch, J.P., 2013. Performing label-fusion-based segmentation using multiple automatically generated templates. Hum. Brain Mapp. 34 (10), 2635–2654. https://doi.org/10.1002/hbm.v34.1010.1002/hbm.22092.

Chen, Z., Wang, J., Lin, F., Dai, H., Mu, K., Zhang, H., 2013. Correlation between lateral geniculate nucleus atrophy and damage to the optic disc in glaucoma. J. Neuroradiol. 40 (4), 281–287. https://doi.org/10.1016/j.neurad.2012.10.004.

Ciccarelli, O., Toosy, A.T., Hickman, S.J., Parker, G.J.M., Wheeler-Kingshott, C.A.M., Miller, D.H., Thompson, A.J., 2005. Optic radiation changes after optic neuritis detected by tractography-based group mapping. Hum. Brain Mapp. 25 (3), 308–316. https://doi.org/10.1002/(ISSN)1097-019310.1002/hbm.v25:310.1002/hbm.20101.

Combes, A.J.E., Matthews, L., Lee, J.S., Li, D.K.B., Carruthers, R., Traboulsee, A.L., Barker, G.J., Palace, J., Kolind, S., 2017. Cervical cord myelin water imaging shows degenerative changes over one year in multiple sclerosis but not neuromyelitis optica spectrum disorder. NeuroImage Clin. 16, 17–22. https://doi.org/10.1016/j.nicl.2017.06.019.

Dai, H., Mu, K.T., Qi, J.P., Wang, C.Y., Zhu, W.Z., Xia, L.M., Chen, Z.Q., Zhang, H., Ai, F., Morelli, J.N., 2011. Assessment of lateral geniculate nucleus atrophy with 3T MR imaging and correlation with clinical stage of glaucoma. Am. J. Neuroradiol. 32 (7), 1347–1353. https://doi.org/10.3174/ajnr.A2486.

Finke, C., Heine, J., Pache, F., Lacheta, A., Borisow, N., Kuchling, J., Bellmann-Strobl, J., Ruprecht, K., Brandt, A.U., Paul, F., 2016. Normal volumes and microstructural integrity of deep gray matter structures in AQP4+ NMOSD. Neurol. Neuroimmunol. Neuroinflamm. 3 (3), e229. https://doi.org/10.1212/NXI.0000000000000229.

Fujita, N., Tanaka, H., Takanashi, M., et al., 2001. Lateral geniculate nucleus: anatomic and functional identification by use of MR imaging. Am. J. Neuroradiol. 22, 1719–1726.

Furlanetto, R.L., Teixeira, S.H., Gracitelli, C.P.B., Lottenberg, C.L., Emori, F., Michelan, M., Amaro, E., Paranhos, A., Bhattacharya, S., 2018. Structural and functional analyses of the optic nerve and lateral geniculate nucleus in glaucoma. PLoS ONE 13 (3), e0194038. https://doi.org/10.1371/journal.pone.0194038.

Gabilondo, I., Martínez-Lapiscina, E.H., Martínez-Heras, E., Fraga-Pumar, E., Llufriu, S., Ortiz, S., Bullich, S., Sepulveda, M., Falcon, C., Berenguer, J., Saiz, A., Sanchez-Dalmau, B., Villoslada, P., 2014. Trans-synaptic axonal degeneration in the visual

pathway in multiple sclerosis. Ann. Neurol. 75 (1), 98–107. https://doi.org/10.1002/ana.24030.
Jarius, S., Wildemann, B., Paul, F., 2014. Neuromyelitis optica: clinical features, immunopathogenesis and treatment. Clin. Exp. Immunol. 176 (2), 149–164. https://doi.org/10.1111/cei.2014.176.issue-210.1111/cei.12271.
Jarius, S., Paul, F., Fechner, K., Ruprecht, K., Kleiter, I., Franciotta, D., Ringelstein, M., Pache, F., Aktas, O., Wildemann, B., 2014. Aquaporin-4 antibody testing: direct comparison of M1-AQP4-DNA-transfected cells with leaky scanning versus M23-AQP4-DNA-transfected cells as antigenic substrate. J. Neuroinflamm. 11 (1), 129. https://doi.org/10.1186/1742-2094-11-129.
Kappos, L., D'Souza, M., Lechner-Scott, J., Lienert, C., 2015. On the origin of neurostatus. Mult. Scler Relat. Disord. 4 (3), 182–185. https://doi.org/10.1016/j.msard.2015.04.001.
Kitajima, M., Hirai, T., Yoneda, T., Iryo, Y., Azuma, M., Tateishi, M., Morita, K., Komi, M., Yamashita, Y., 2015. Visualization of the medial and lateral geniculate nucleus on phase difference enhanced imaging. Am. J. Neuroradiol. 36 (9), 1669–1674. https://doi.org/10.3174/ajnr.A4356.
Lennon, V.A., Wingerchuk, D.M., Kryzer, T.J., Pittock, S.J., Lucchinetti, C.F., Fujihara, K., Nakashima, I., Weinshenker, B.G., 2004. A serum autoantibody marker of neuromyelitis optica: distinction from multiple sclerosis. Lancet Lond. Engl. 364 (9451), 2106–2112. https://doi.org/10.1016/S0140-6736(04)17551-X.
Magon, S., Chakravarty, M.M., Amann, M., Weier, K., Naegelin, Y., Andelova, M., Radue, E.-W., Stippich, C., Lerch, J.P., Kappos, L., Sprenger, T., 2014. Label-fusion-segmentation and deformation-based shape analysis of deep gray matter in multiple sclerosis: the impact of thalamic subnuclei on disability. Hum. Brain Mapp. 35 (8), 4193–4203. https://doi.org/10.1002/hbm.v35.810.1002/hbm.22470.
Magon, S., Tsagkas, C., Gaetano, L., Patel, R., Naegelin, Y., Amann, M., Parmar, K., Papadopoulou, A., Wuerfel, J., Stippich, C., Kappos, L., Chakravarty, M.M., Sprenger, T., 2020. Volume loss in the deep gray matter and thalamic subnuclei: a longitudinal study on disability progression in multiple sclerosis. J. Neurol. 267 (5), 1536–1546. https://doi.org/10.1007/s00415-020-09740-4.
Manogaran, P., Vavasour, I.M., Lange, A.P., Zhao, Y., McMullen, K., Rauscher, A., Carruthers, R., Li, D.K.B., Traboulsee, A.L., Kolind, S.H., 2016. Quantifying visual pathway axonal and myelin loss in multiple sclerosis and neuromyelitis optica. NeuroImage Clin. 11, 743–750. https://doi.org/10.1016/j.nicl.2016.05.014.
Matthews, L., Kolind, S., Brazier, A., Leite, M.I., Brooks, J., Traboulsee, A., Jenkinson, M., Johansen-Berg, H., Palace, J., Bradl, M., 2015. Imaging surrogates of disease activity in neuromyelitis optica allow distinction from multiple sclerosis. PLoS ONE 10 (9), e0137715. https://doi.org/10.1371/journal.pone.0137715.
Oertel, F.C., Kuchling, J., Zimmermann, H., Chien, C., Schmidt, F., Knier, B., Bellmann-Strobl, J., Korn, T., Scheel, M., Klistorner, A., Ruprecht, K., Paul, F., Brandt, A.U., 2017. Microstructural visual system changes in AQP4-antibody-seropositive NMOSD. Neurol. Neuroimmunol. Neuroinflamm. 4 (3), e334. https://doi.org/10.1212/NXI.0000000000000334.
Oertel, F.C., Havla, J., Roca-Fernández, A., Lizak, N., Zimmermann, H., Motamedi, S., Borisow, N., White, O.B., Bellmann-Strobl, J., Albrecht, P., Ruprecht, K., Jarius, S., Palace, J., Leite, M.I., Kuempfel, T., Paul, F., Brandt, A.U., 2018. Retinal ganglion cell loss in neuromyelitis optica: a longitudinal study. J. Neurol. Neurosurg. Psychiatry 89 (12), 1259–1265. https://doi.org/10.1136/jnnp-2018-318382.
Oertel, F.C., Zimmermann, H., Paul, F., Brandt, A.U., 2018. Optical coherence tomography in neuromyelitis optica spectrum disorders: potential advantages for individualized monitoring of progression and therapy. EPMA J. 9 (1), 21–33. https://doi.org/10.1007/s13167-017-0123-5.
Papadopoulou, A., Gaetano, L., Pfister, A., Altermatt, A., Tsagkas, C., Morency, F., Brandt, A.U., Hardmeier, M., Chakravarty, M.M., Descoteaux, M., Kappos, L., Sprenger, T., Magon, S., 2019. Damage of the lateral geniculate nucleus in MS: assessing the missing node of the visual pathway. Neurology 92 (19), e2240–e2249. https://doi.org/10.1212/WNL.0000000000007450.
Papadopoulou, A., Oertel, F.C., Gaetano, L., Kuchling, J., Zimmermann, H., Chien, C., Siebert, N., Asseyer, S., Bellmann-Strobl, J., Ruprecht, K., Chakravarty, M.M., Scheel, M., Magon, S., Wuerfel, J., Paul, F., Brandt, A.U., 2019. Attack-related damage of thalamic nuclei in neuromyelitis optica spectrum disorders. J. Neurol. Neurosurg. Psychiatry Published Online First 90 (10), 1156–1164. https://doi.org/10.1136/jnnp-2018-320249.
Paul, F., Jarius, S., Aktas, O., Bluthner, M., Bauer, O., Appelhans, H., Franciotta, D., Bergamaschi, R., Littleton, E., Palace, J., Seelig, H.-P., Hohlfeld, R., Vincent, A., Zipp, F., Lassmann, H., 2007. Antibody to aquaporin 4 in the diagnosis of neuromyelitis optica. PLoS Med. 4 (4), e133. https://doi.org/10.1371/journal.pmed.0040133.
Petzold, A., Wattjes, M.P., Costello, F., Flores-Rivera, J., Fraser, C.L., Fujihara, K., Leavitt, J., Marignier, R., Paul, F., Schippling, S., Sindic, C., Villoslada, P., Weinshenker, B., Plant, G.T., 2014. The investigation of acute optic neuritis: a review and proposed protocol. Nat. Rev. Neurol. 10 (8), 447–458. https://doi.org/10.1038/nrneurol.2014.108.
Pfueller, C.F., Paul, F., 2011. Imaging the visual pathway in neuromyelitis optica. Mult. Scler. Int. 2011, 1–5. https://doi.org/10.1155/2011/869814.
Pichiecchio, A., Tavazzi, E., Poloni, G., Ponzio, M., Palesi, F., Pasin, M., Piccolo, L., Tosello, D., Romani, A., Bergamaschi, R., Piccolo, G., Bastianello, S., 2012. Advanced magnetic resonance imaging of neuromyelitis optica: a multiparametric approach. Mult. Scler. Houndmills Basingstoke Engl. 18 (6), 817–824. https://doi.org/10.1177/1352458511431072.
R Core Team, 2017. R: A Language and Environment for Statistical Computing. R Foundation for Statistical Computing, Vienna, Austria https://www.r-project.org/ (accessed 23 Nov 2018).
Rocca, M.A., Mesaros, S., Preziosa, P., Pagani, E., Stosic-Opincal, T., Dujmovic-Basuroski, I., Drulovic, J., Filippi, M., 2013. Wallerian and trans-synaptic degeneration contribute to optic radiation damage in multiple sclerosis: a diffusion tensor MRI study. Mult. Scler Houndmills Basingstoke Engl. 19 (12), 1610–1617. https://doi.org/10.1177/1352458513485146.
Smith, S.M., Zhang, Y., Jenkinson, M., Chen, J., Matthews, P.M., Federico, A., De Stefano, N., 2002. Accurate, robust, and automated longitudinal and cross-sectional brain change analysis. NeuroImage 17 (1), 479–489.
Stadelmann, C., 2011. Multiple sclerosis as a neurodegenerative disease: pathology, mechanisms and therapeutic implications. Curr. Opin. Neurol. 24, 224–229. https://doi.org/10.1097/WCO.0b013e328346056f.
Tian, D.-C., Su, L., Fan, M., Yang, J., Zhang, R., Wen, P., Han, Y., Yu, C., Zhang, C., Ren, H., Shi, K., Zhu, Z., Dong, Y., Liu, Y., Shi, F.-D., 2018. Bidirectional degeneration in the visual pathway in neuromyelitis optica spectrum disorder (NMOSD). Mult. Scler Houndmills Basingstoke Engl. 24 (12), 1585–1593. https://doi.org/10.1177/1352458517727604.
Wingerchuk, D.M., Pittock, S.J., Lucchinetti, C.F., Lennon, V.A., Weinshenker, B.G., 2007. A secondary progressive clinical course is uncommon in neuromyelitis optica. Neurology 68 (8), 603–605. https://doi.org/10.1212/01.wnl.0000254502.87233.9a.
Wingerchuk, D.M., Banwell, B., Bennett, J.L., Cabre, P., Carroll, W., Chitnis, T., de Seze, J., Fujihara, K., Greenberg, B., Jacob, A., Jarius, S., Lana-Peixoto, M., Levy, M., Simon, J.H., Tenembaum, S., Traboulsee, A.L., Waters, P., Wellik, K.E., Weinshenker, B.G., 2015. International consensus diagnostic criteria for neuromyelitis optica spectrum disorders. Neurology 85 (2), 177–189. https://doi.org/10.1212/WNL.0000000000001729.